

Supplement of Hydrol. Earth Syst. Sci., 19, 4215–4228, 2015
<http://www.hydrol-earth-syst-sci.net/19/4215/2015/>
doi:10.5194/hess-19-4215-2015-supplement
© Author(s) 2015. CC Attribution 3.0 License.



Hydrology and
Earth System
Sciences

Open Access



Supplement of

High-quality observation of surface imperviousness for urban runoff modelling using UAV imagery

P. Tokarczyk et al.

Correspondence to: P. Tokarczyk (piotr.tokarczyk@gmail.com)

The copyright of individual parts of the supplement might differ from the CC-BY 3.0 licence.

720 **Supplement**

S1 Remote sensing methods to extract the imperviousness maps

A considerable amount of remote sensing research has been devoted to the problem of mapping impervious surfaces. Here, we review some of the previous studies and evaluate them in respect of the datasets and classification methods. Furthermore, we focus on the studies which use the classified
725 land-use to predict urban rainfall runoff.

Whereas few studies have used low-resolution (GSD > 100m) satellite sensors, such as MODIS (Lu et al., 2008; Boegh et al., 2009), AVHRR (Carlson and Arthur, 2000) and DMSP-OLS (Elvidge et al., 2007; Lu et al., 2008), the large part of the research in this area focused on medium and high spatial resolution satellite data. Because of its exceptional temporal resolution, Landsat is still the most
730 popular satellite platform. A large number of authors used Landsat 5 TM (Civco et al., 2002; Carlson, 2004; Bauer et al., 2008; Yuan and Bauer, 2006; Li et al., 2011; Parece and Campbell, 2013; Dougherty et al., 2004) and Landsat 7 ETM+ data (Civco et al., 2002; Yang et al., 2003; Wu and Murray, 2003; Lu and Weng, 2006; Lee and Lathrop, 2006; Powell et al., 2007; Chormanski et al., 2008; Chabaeva et al., 2009; Van de Voorde et al., 2009) for analysing impervious surface cover.
735 Other examples of using images acquired by high resolution platforms include SPOT (Yang et al., 2009; Li et al., 2011; Tan et al., 2009) and ASTER (Weng and Hu, 2008; Hu and Weng, 2009; Weng et al., 2009).

However, recent developments of remote sensing imaging sensors and platforms gave access to VHR imagery. Examples of VHR satellite sensors application to impervious surfaces mapping include Ikonos (Cablak and Minor, 2003; Lu and Weng, 2009; Mohapatra et al., 2008; Chormanski et al., 2008; Van de Voorde et al., 2009; Mathieu et al., 2007), and QuickBird (Lu et al., 2008; Yuan and Bauer, 2006; Zhou and Wang, 2008). Except of satellite imagery, aerial images are also an important source of information. Many studies used aerial orthophotos only as a reference check to satellite imagery (Yang et al., 2003; DeBusk et al., 2010; Parece and Campbell, 2013). However
740 few attempts to automatically map imperviousness using such data were made (Nielsen et al., 2011; Dougherty et al., 2004; Hodgson et al., 2003; Zhou and Wang, 2008; Fankhauser, 1999; Lee and Heaney, 2003).

One possible way to extract imperviousness from images is to interpret them manually. Even though this is the most reliable method, and has been used in few studies (*e.g.* Lee and Heaney
750 (2003)), it is very costly in terms of time and money. Therefore it is common to automate the process by using image classification. Maybe the simplest method is to assume that only vegetation is pervious and rely on the normalized differential vegetation index (NDVI) (Nielsen et al., 2011; Carlson and Arthur, 2000). Many of the studies use more advanced classification methods, such as object based image analysis (OBIA) (Zhou and Wang, 2008; Hodgson et al., 2003; Nielsen et al.,
755 2011; Mathieu et al., 2007). Other examples include maximum likelihood classifier (Fankhauser,

1999; Hodgson et al., 2003), spectral mixture analysis (SMA) (Small, 2003; Van de Voorde et al., 2009; Weng et al., 2009), artificial neural networks (ANN) (Chormanski et al., 2008; Van de Voorde et al., 2009; Lee and Lathrop, 2006), classification and regression trees (CART) (Yang et al., 2003; Li et al., 2011; Dougherty et al., 2004) and rule-based classifiers (Hodgson et al., 2003). Some
 760 of the mentioned methods also use the perviousness maps for urban drainage modelling like we do (Nielsen et al., 2011; Melesse and Wang, 2008; Chormanski et al., 2008; Dougherty et al., 2004; Lee and Heaney, 2003; Fankhauser, 1999). However, to our best knowledge no studies exist, that used UAV-based imagery to extract imperviousness information, and to use it in the field of urban drainage modelling.

765 **S2 UAV platform**

The UAV platform used in this study is an autonomous fixed-wing drone produced by senseFly SA (*cf.* <http://www.senseFly.com>). Table S1 includes detailed information about the platform.

Weight (incl. camera)	ca. 0.69 kg
Wingspan	96 cm
Material	EPP foam, carbon structure and composite parts
Propulsion	Electric pusher propeller, 160 W brushless DC motor
Battery	11.1 V, 2150 mAh
Camera (supplied)	16 MP IXUS/ELPH
Cameras (oprional)	S110 RGB, thermoMAP
Max. flight time	50 min
Nominal speed	40-90 km/h
Wind resistance	Up to 45 km/h (12 m/s)
Radio link range	Up to 3 km
Max. coverage (single flight)	Up to 12 km ²
Cost	ca. 20'000 CHF (Drone + Software)

Table S1. Specifications of the UAV used in the study (source: <http://www.senseFly.com>)

The imaging unit mounted on a UAV was a customized version of Canon IXUS 127 HS compact
 770 camera. Table S2 includes its specifications.

Camera effective pixels	ca. 16.1 million
Lens' focal length	4.3 - 21.5 mm (35 mm equivalent: 24 - 120 mm)
Interfaces	Hi-speed USB, HDMI Output, Analog audio output, Analog video output (NTSC/PAL)
Dimensions	93.2 × 57.0 × 20.0 mm
Weight	ca. 135 g (incl. battery and memory card)

Table S2. Specifications of the Canon IXUS 127 HS Camera

S3 Exploratory data analysis of the importance of image source and processing method for the surface runoff

S3.1 Regression

775 **Imperviousness**

Please refer to Table S3 and Figure S3.

Here we try to answer a following question: Which has the greater influence/is stronger correlate with a change in imperviousness and surface runoff characteristics, the image source or the processing method?
780

Model and results

Here we present logit-transformation of imperviousness. This was done to constrain the model output to the range between 0 and 1 and not to improve the statistical assumptions regarding the errors
785 of the data generating process.

Description/Interpretation

UAV images seem to be negatively correlated with the imperviousness. The effect is not really strong. Regarding the methods, there seems to be no influence, because the estimated linear relation is practically negligible. In addition, there is no evidence for interactions between the image source and the processing method.
790

Peak runoff

795 *Model and results*

Please refer to Table S4 and Figure S4

Description/Interpretation

800 UAVdata generally seem to produce slightly smaller peaks, whereas the RQE method is positively correlated to peak hight. However both effects are not significant by any means. There are no interactions of these two. Statistical assumptions are not fulfilled.

Runoff volume

805

Model and results

Please refer to Table S5 and Figure S5

Description/Interpretation

810 UAV data generally seem to produce slightly runoff volumes, whereas the RQE method is positively correlated to runoff volume. However both effects are not significant by any means. There are no interactions of these two. Statistical assumptions are not fulfilled.

815 **Time to peak**

Analysis was not performed, because exploratory analysis suggest that the differences between the different image sources are negligibly small.

820

S4 Pipe flow predictions

Please refer to Figure S6

Acknowledgements. This publication is an outcome of a fruitful interdisciplinary collaboration between photogrammetrists and hydrologists, which was triggered by joint supervision of Matthew Moy de Vitry's Master thesis titled: "Improving Urban Flood Management with Autonomous Mini-UAVs". We would like to thank 825 Matthew for providing us with a UAV dataset. Also, we are very grateful to MeteoSwiss and the city of Lucerne for providing us with the precipitation and infrastructure data, and Holinger company for providing us with the *swisstopo* aerial image data. Last but not least, we would like to thank Philippe Gerber for helping us with an automatic calibration of pipe flow model.

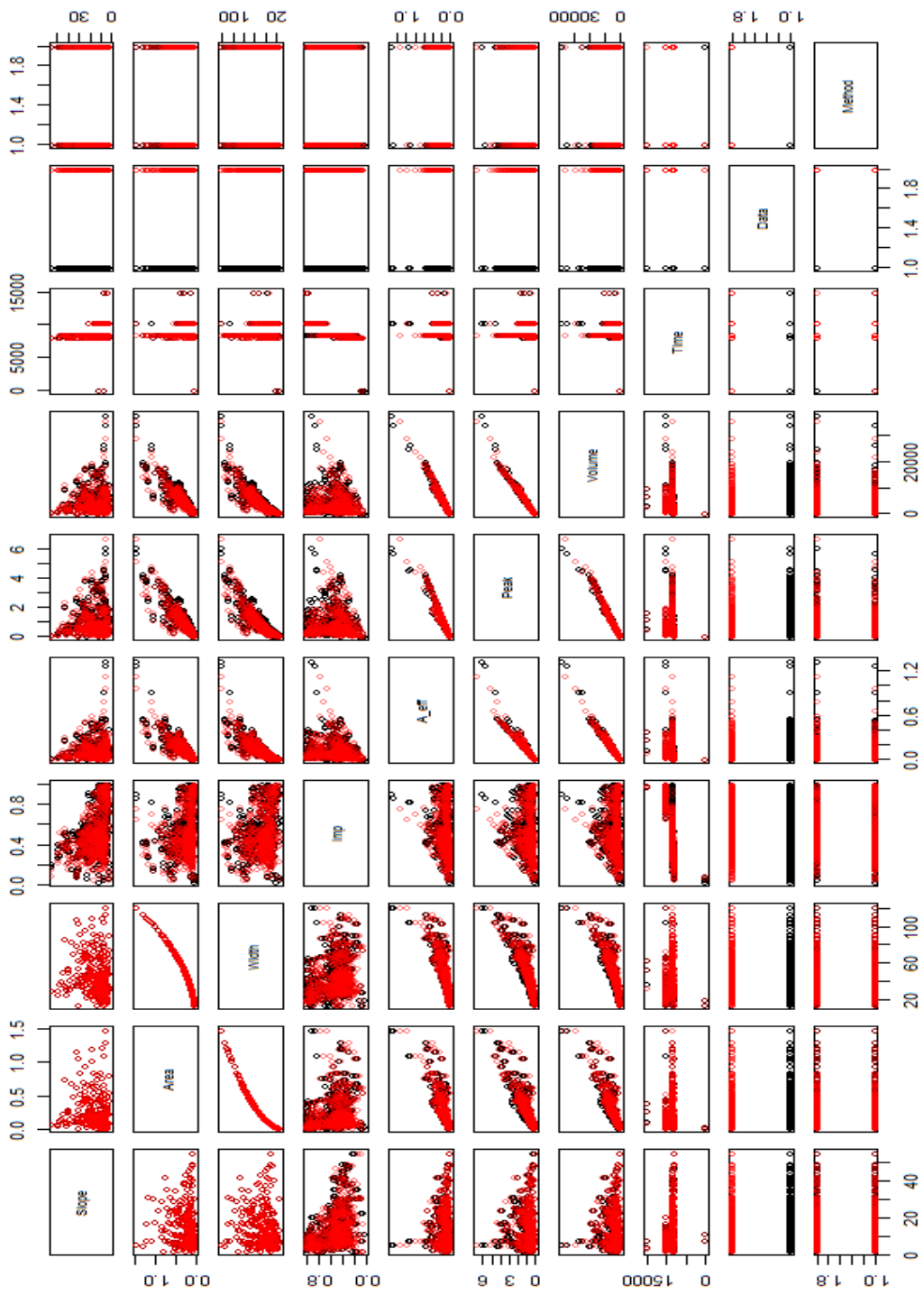


Figure S1. Scatterplot of surface runoff characteristics for the 307 individual subcatchments of the WarteggSWMM model. Black = Orthophotos, Red= UAV images. A_eff: effective area, Imp: imperviousness

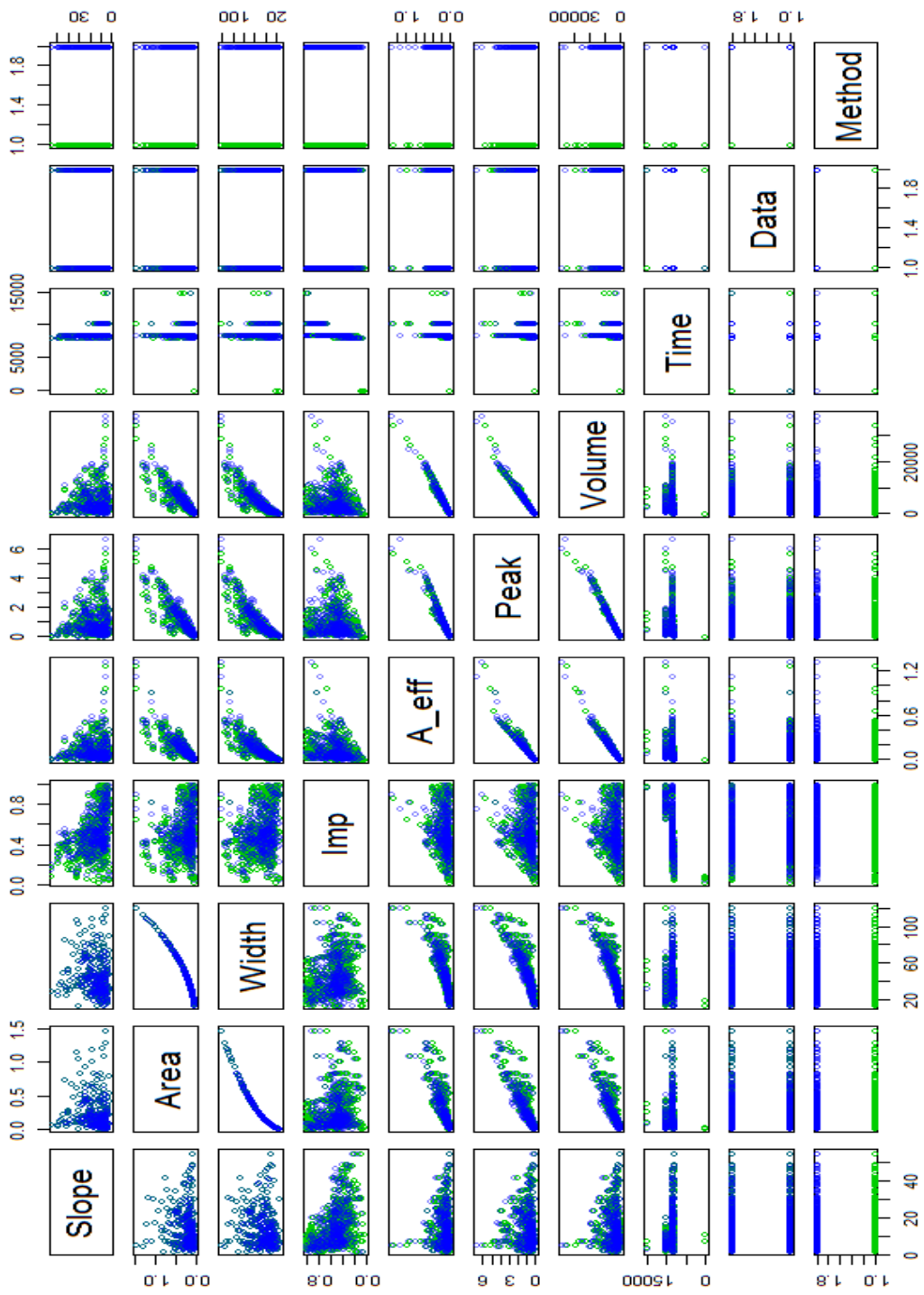


Figure S2. Scatterplot of surface runoff characteristics for the 307 individual subcatchments of the WarteggSWMM model. Green= ML, Blue = RQE. A_eff: effective area, Imp: imperviousness

Table S3. Summary results of the regression analysis. The negative sign of the estimated slope parameter suggests that the UAV images generally go together with a lower imperviousness. In addition, the influence of the image source seems to be larger than that of the classification method, although the high p-values for all parameters suggest that it is not very likely that the observed values of imperviousness were to have occurred under the given statistical model.

<i>Dependent variable:</i>	
	Volume
DataUAV	-301.699 (331.033)
MethodRQE	298.671 (331.033)
DataUAV:MethodRQE	199.362 (468.151)
Constant	3,893.406*** (234.075)
Observations	1,228
R ²	0.003
Adjusted R ²	0.001
Residual Std. Error	4,101.333 (df = 1224)
F Statistic	1.274 (df = 3; 1224)

Note: *p<0.1; **p<0.05; ***p<0.01

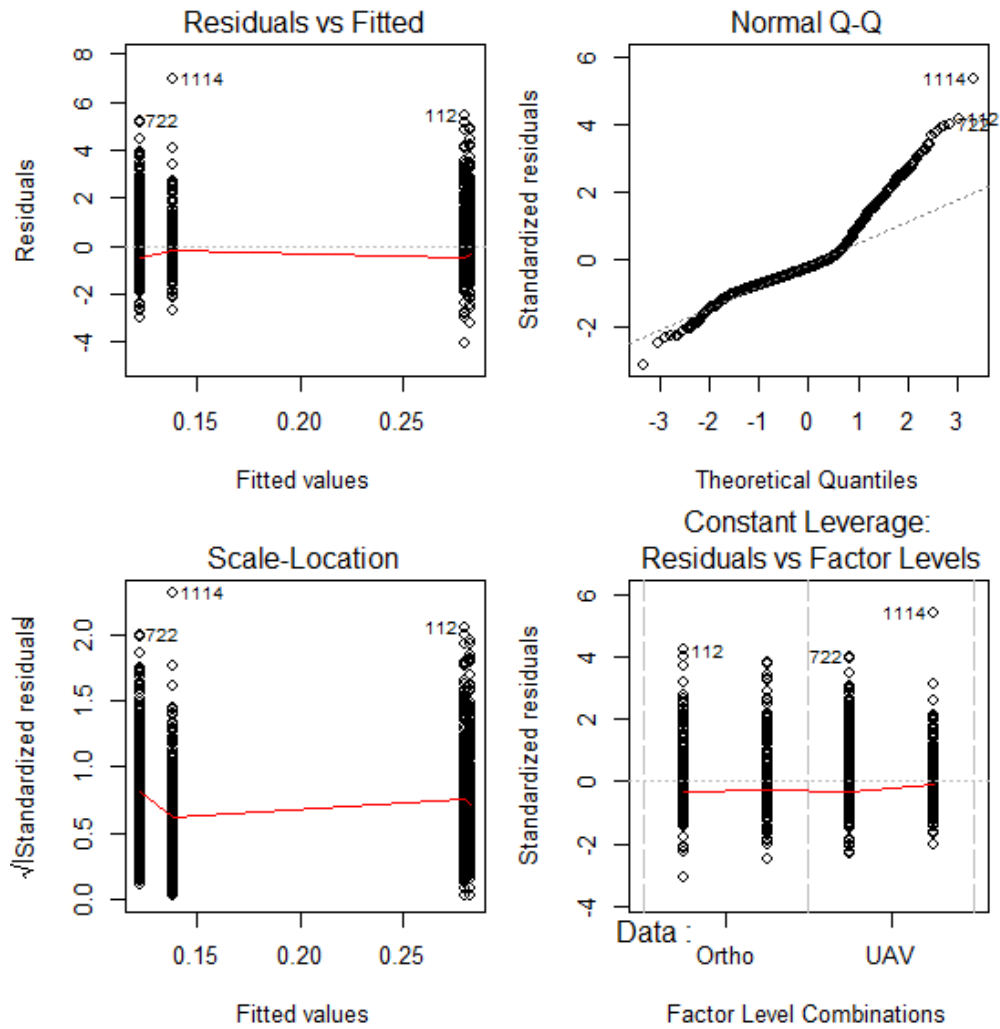


Figure S3. Diagnostic plots of the regression analysis. It is obvious that the statistical assumptions are not fulfilled very well and that the observe imperviousness is not well explained.

Table S4. Summary results of the regression analysis for peak runoff. The negative sign of the estimated slope parameter suggests that the UAV images generally go together with a lower stormwater peak flow. Here, the influence of the image source seems to be in the same order of magnitude than that of the classification method, although the former is negatively correlated and the latter has a positive correlation with peak runoff. Again, the high p-values for all parameters suggest that it is not very likely that the observed peak runoff values were to have occurred under the given statistical model.

<i>Dependent variable:</i>	
	Peak
DataUAV	-0.065 (0.067)
MethodRQE	0.068 (0.067)
DataUAV:MethodRQE	0.038 (0.094)
Constant	0.826*** (0.047)
Observations	1,228
R ²	0.004
Adjusted R ²	0.001
Residual Std. Error	0.827 (df = 1224)
F Statistic	1.507 (df = 3; 1224)

Note: *p<0.1; **p<0.05; ***p<0.01

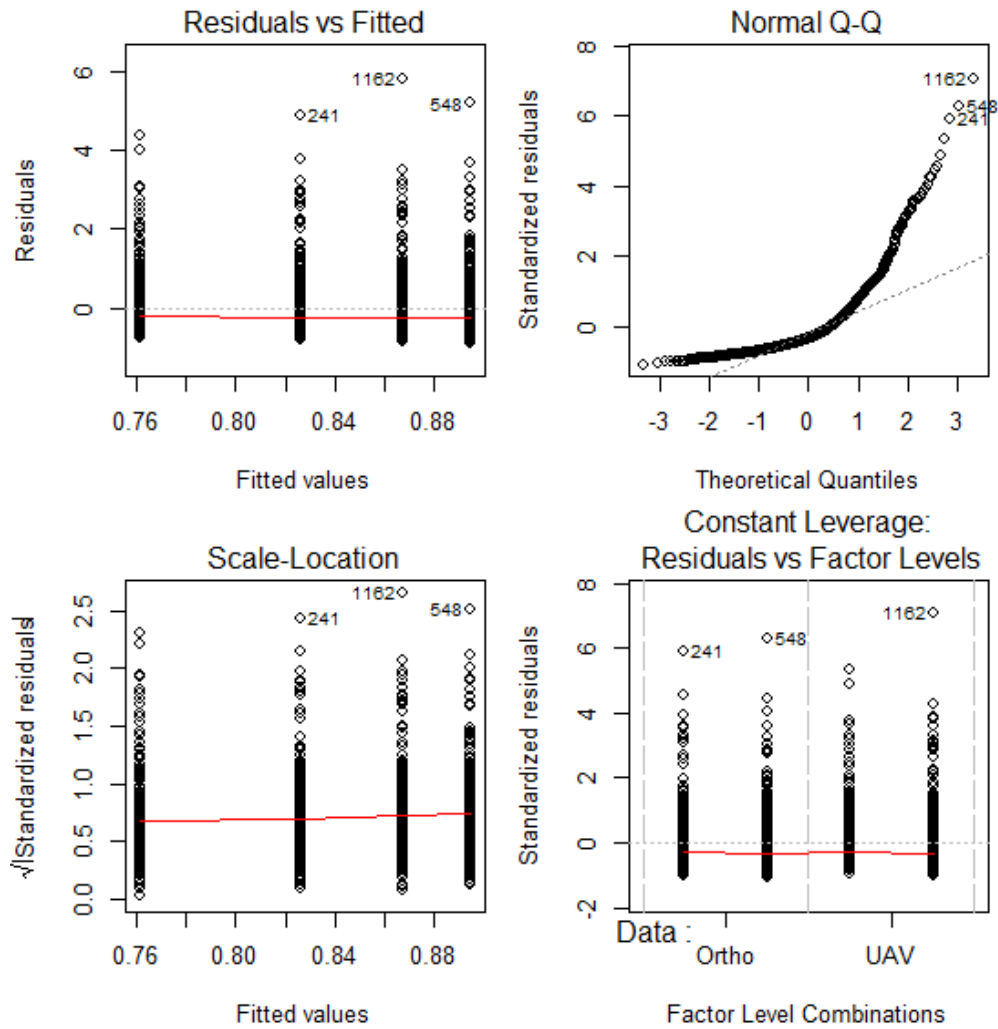


Figure S4. Diagnostic plots of the regression analysis. It is obvious that the statistical assumptions are not fulfilled very well and that the observe imperviousness is not well explained.

Table S5. Summary results of the regression analysis for runoff volume.

<i>Dependent variable:</i>	
	Volume
DataUAV	−301.699 (331.033)
MethodRQE	298.671 (331.033)
DataUAV:MethodRQE	199.362 (468.151)
Constant	3,893.406*** (234.075)
Observations	1,228
R ²	0.003
Adjusted R ²	0.001
Residual Std. Error	4,101.333 (df = 1224)
F Statistic	1.274 (df = 3; 1224)

Note: *p<0.1; **p<0.05; ***p<0.01

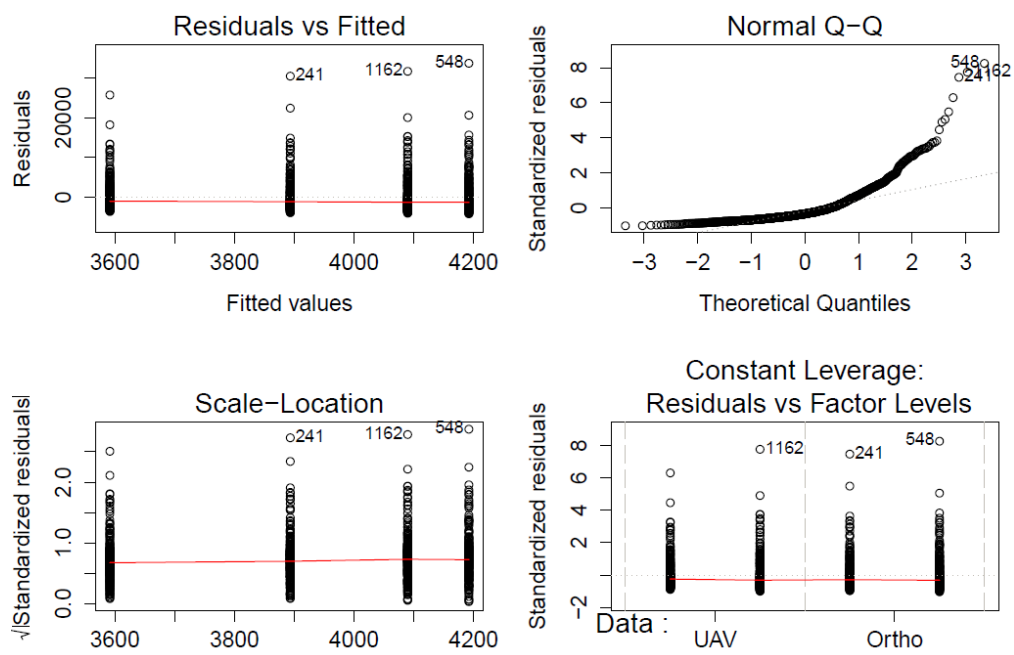


Figure S5. Diagnostic plots of the regression analysis. It is obvious that the statistical assumptions are not fulfilled very well and that the observe imperviousness is not well explained.

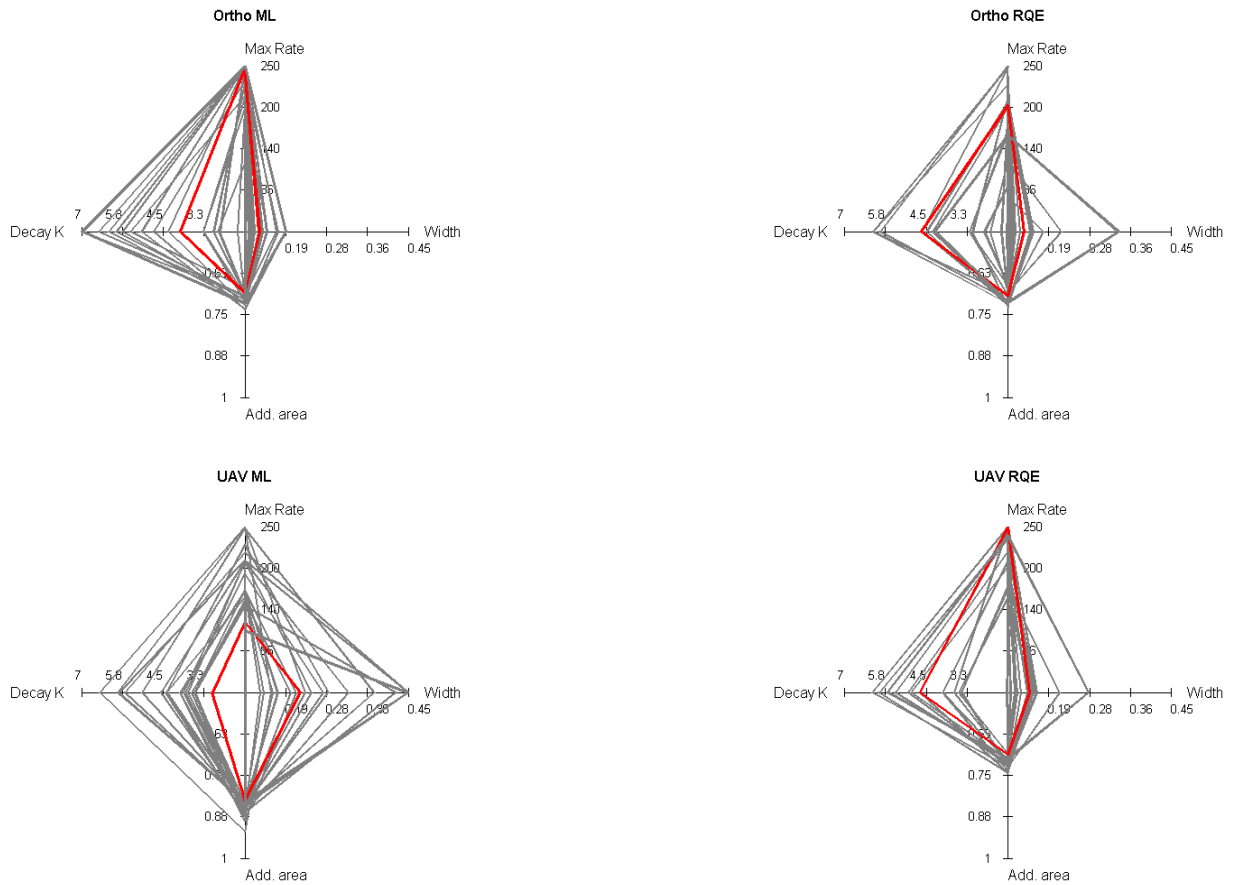


Figure S6. Distribution of calibration parameter (Decay K: infiltration decay rate after HORTON; MaxRate: maximum infiltration rate after HORTON; width: conceptual parameter describing the width of a subcatchment; Add.area: conceptual parameter describing event-based sewer infiltration) values identified during the auto-calibration process. Grey rhombs represent the optimum parameter set identified for each population; the red rhomb represents the final parameter set.